

# Optimizing relativistic energy density functionals: covariance analysis

T. Nikšić<sup>1</sup>, N. Paar<sup>1</sup>, P.-G. Reinhard<sup>2</sup>, D. Vretenar<sup>1</sup>

<sup>1</sup>Physics Department, Faculty of Science, University of Zagreb, Zagreb/Croatia

<sup>2</sup>Institut für Theoretische Physik, Universität Erlangen/Nürnberg,  
Erlangen/Germany

**Abstract.** The stability of model parameters for a class of relativistic energy density functionals, characterized by contact (point-coupling) effective inter-nucleon interactions and density-dependent coupling parameters, is analyzed using methods of statistical analysis. A set of pseudo-observables in infinite and semi-infinite nuclear matter is used to define a quality measure  $\chi^2$  for subsequent analysis. We calculate uncertainties of model parameters and correlation coefficients between parameters, and determine the eigenvectors and eigenvalues of the matrix of second derivatives of  $\chi^2$  at the minimum. This allows to examine the stability of the density functional in nuclear matter, and to deduce weakly and strongly constrained combinations of parameters. In addition, we also compute uncertainties of observables that are not included in the calculation of  $\chi^2$ : binding energy of asymmetric nuclear matter, surface thickness of semi-infinite nuclear matter, binding energies and charge radii of finite nuclei.

## 1. Introduction

This special issue is devoted to model analysis in connection with least-squares ( $\chi^2$ ) fits and subsequent statistical analysis [1]. We will use these techniques to explore the details of a particular class of the relativistic mean field model (RMF), namely the density-dependent point-coupling model DD-PC1 [2]. The RMF, similar as its non-relativistic counterparts Skyrme-Hartree-Fock (SHF) and Gogny force [3], belongs to the family of self-consistent nuclear models based either on effective interactions or nuclear energy density functionals. These models necessitate calibration of the model parameters to empirical data, usually bulk properties of nuclear ground states. In the early days of RMF models coupling and mass parameters were determined basically by an intuitive search [4]. A first systematic calibration using a straightforward  $\chi^2$ -fit was performed in Ref. [5]. The fitting protocol and data pool were similar to those applied within the SHF framework [6]. Since then RMF parameterisations have been significantly improved by including more and more data in the data pool (for reviews see Refs. [7, 8, 9, 10]). The traditional RMF approach was based on nucleon-meson couplings, that is, on finite-range effective interactions. An alternative is the point-coupling (PC) RMF which is closer in spirit to the non-relativistic SHF approach and allows a simpler treatment of exchange terms. It was first introduced in [11] and, by performing  $\chi^2$  fits of model parameters [12], its performance has been improved to match the level of traditional RMF models. A significant step forward in the flexibility of RMF models was the introduction of an explicit density dependence of coupling parameters [13]. This idea was later used also in the PC-RMF approach, and an empirical ansatz for the density dependence of the nucleon-vertex parameters was employed in the formulation of the functional DD-PC1 [2], which will be the basis of the present study.

Although one could consider different classes of RMF models for the statistical analysis [14, 15], in this work we explore the intrinsic structure of one particular model, i.e. the functional DD-PC1. We follow the strategy of the model study [16] that used pseudo-data related to infinite nuclear matter to generate a  $\chi^2$  measure, which was then analyzed according to the rules of statistical analysis. This procedure provides theoretical uncertainties for both model parameters and predicted observables. The results of the present investigation are general and can also be applied to other classes of the RMF models because, by analyzing the inter-dependencies between the couplings, one is able to determine strongly and weakly constrained combinations of model parameters and estimate their impact in extrapolating uncertainties.

## 2. Covariance analysis

Following the notation of Ref. [17], we denote a point in an  $F$ -dimensional parameter space by  $\mathbf{p} = \{p_1, \dots, p_F\}$  and, therefore, each value of  $\mathbf{p}$  corresponds to a particular model. Model parameters are usually adjusted to ground-state properties of a selected set of finite nuclei, and occasionally also to bulk empirical properties of infinite nuclear

matter. A calibration of model parameters starts with defining a quality measure:

$$\chi^2(\mathbf{p}) = \sum_{n=1}^N \left( \frac{\mathcal{O}_n^{(th)}(\mathbf{p}) - \mathcal{O}_n^{(exp)}}{\Delta\mathcal{O}_n} \right)^2, \quad (1)$$

where  $N$  is the number of observables  $\hat{\mathcal{O}}_n$  considered in the analysis, *(th)* and *(exp)* denote theoretical and experimental values, respectively. Every observable is weighted by the inverse of  $\Delta\mathcal{O}_n$  which, in fits to experimental results, is typically associated with the accuracy of the measurement. In calibrating a model one often uses an ‘‘adopted error’’ which is supposed to include all sources of uncertainty and is adjusted in such a way that  $\chi^2(\mathbf{p}_0) \approx N - F$  [1, 18]. The optimal set  $\mathbf{p}_0$ , that is, the ‘‘best model’’ corresponds to the minimum of  $\chi^2$  on the multidimensional parameter surface, and this implies that all first derivatives of the function  $\chi^2$  vanish at  $\mathbf{p}_0$ :

$$\left. \frac{\partial\chi^2(\mathbf{p})}{\partial p_i} \right|_{\mathbf{p}=\mathbf{p}_0} = 0, \quad \forall i = 1, \dots, F. \quad (2)$$

Moreover, the symmetric  $F \times F$  matrix of second derivatives  $\partial^2\chi^2/(\partial p_i\partial p_j)$  has to be positive-definite at  $\mathbf{p}_0$ . To analyze the deviation of  $\chi^2$  from its minimum value, it is convenient to define dimensionless parameters

$$x_i = \frac{(\mathbf{p} - \mathbf{p}_0)_i}{(\mathbf{p}_0)_i}. \quad (3)$$

The minimum is then determined by  $\mathbf{x} = 0$ . In the vicinity of the minimum  $\chi^2$  can be represented by a Taylor series expansion. The lowest-order (quadratic) deviation of  $\chi^2$  reads

$$\Delta\chi^2(\mathbf{x}) = \chi^2(\mathbf{p}) - \chi^2(\mathbf{p}_0) = \mathbf{x}^T \hat{\mathcal{M}} \mathbf{x}, \quad (4)$$

$$\mathcal{M}_{ij} = \frac{1}{2} \left. \frac{\partial^2\chi^2}{\partial x_i\partial x_j} \right|_{\mathbf{x}=0} = \frac{1}{2} (\mathbf{p}_0)_i (\mathbf{p}_0)_j \partial_i \partial_j \chi^2(\mathbf{p}_0). \quad (5)$$

The curvature matrix  $\hat{\mathcal{M}}$  is symmetric and can be diagonalized by an orthogonal transformation  $\hat{\mathcal{M}} = \hat{\mathcal{A}} \hat{\mathcal{D}} \hat{\mathcal{A}}^T$ , where  $\hat{\mathcal{A}}$  denotes the orthogonal matrix with columns corresponding to normalised eigenvectors of  $\hat{\mathcal{M}}$ , and the diagonal matrix  $\hat{\mathcal{D}}$  contains the eigenvalues of  $\hat{\mathcal{M}}$ . The deviation of  $\chi^2$  from its minimum value can therefore be expressed as [16]

$$\Delta\chi^2(\mathbf{x}) = \mathbf{x}^T (\hat{\mathcal{A}} \hat{\mathcal{D}} \hat{\mathcal{A}}^T) \mathbf{x} = \xi^T \mathcal{D} \xi = \sum_{i=1}^F \lambda_i \xi_i^2. \quad (6)$$

The transformed vectors  $\xi = \hat{\mathcal{A}}^T \mathbf{x}$  define the principal axes on the  $F$ -dimensional surface in parameter space. Soft directions are characterized by small eigenvalues  $\lambda_i$ , that is, there is very little deterioration in the function  $\chi^2$  as one moves along a direction defined by the eigenvector that corresponds to a small eigenvalue of  $\hat{\mathcal{M}}$ . This implies that the corresponding linear combinations of model parameters are badly constrained by the observables included in the  $\chi^2$  adjustment. On the other hand, stiff directions are characterized by large eigenvalues  $\lambda_i$ , that is, the function  $\chi^2$  increases rapidly

along these directions and the corresponding linear combinations of parameters are tightly constrained by the observables that determine the  $\chi^2$  measure. A survey of the eigenvalues  $\lambda_i$  and eigenvectors  $\xi_i$  of  $\hat{\mathcal{M}}$  for the relativistic functional DD-PC1 presents the major part of the analysis performed in this work.

Another important concept in statistical analysis is the covariance between two observables  $A$  and  $B$  [1, 17, 18]:

$$\text{cov}(A, B) = \sum_{i,j=1}^F \frac{\partial A}{\partial x_i} (\mathcal{M}^{-1})_{ij} \frac{\partial B}{\partial x_j} = \sum_{i=1}^F \frac{\partial A}{\partial \xi_i} \lambda_i^{-1} \frac{\partial B}{\partial \xi_i}, \quad (7)$$

from which one defines the correlation coefficient

$$\rho(A, B) = \frac{\text{cov}(A, B)}{\sqrt{\text{var}(A)\text{var}(B)}}, \quad (8)$$

and where the variance of an observable is simply:  $\text{var}(A) = \text{cov}(A, A)$ . The observables  $A$  and  $B$  are fully correlated if  $\rho(A, B) = 1$ , anti-correlated if  $\rho(A, B) = -1$ , and independent if  $\rho(A, B) = 0$ .

For the calculation of covariances with Eq. (7), one has to compute derivatives of observables with respect to model parameters. Here we use the Richardson extrapolation method [19] for the numerical calculation of derivatives and define the  $m$ -th order expression

$$G_m(h) = \frac{4^m G_{m-1}(h/2) - G_{m-1}(h)}{4^m - 1}, \quad m = 1, 2, \dots, \quad (9)$$

where

$$G_0(h) = \frac{1}{2h} [f(a+h) - f(a-h)] \quad (10)$$

is a simple first-order finite difference, and thus  $f'(a) - G_m(h) = O(h^{2(m+1)})$ . As in the recent analysis of the propagation of uncertainties in Skyrme energy density functionals of Ref. [20], here we extrapolate up to  $m = 2$  in the computation of derivatives with respect to model parameters.

### 3. The Relativistic Density Functional DD-PC1

The basic building blocks of a relativistic nuclear energy density functional are the densities and currents bilinear in the Dirac spinor field  $\psi$  of the nucleon:  $\bar{\psi} \mathcal{O}_\tau \Gamma \psi$ , with  $\mathcal{O}_\tau \in \{1, \tau_i\}$  and  $\Gamma \in \{1, \gamma_\mu, \gamma_5, \gamma_5 \gamma_\mu, \sigma_{\mu\nu}\}$ . Here  $\tau_i$  are the isospin Pauli matrices and  $\Gamma$  generically denotes the Dirac matrices. A general covariant Lagrangian can be written as a power series in the currents  $\bar{\psi} \mathcal{O}_\tau \Gamma \psi$  and their derivatives. The point-coupling functional or point-coupling relativistic mean-field (PC-RMF) model is structurally particularly simple as it involves only contact couplings between these currents. Actually we take into account the following channels: isoscalar-scalar  $(\bar{\psi}\psi)^2$ , isoscalar-vector

$(\bar{\psi}\gamma_\mu\psi)(\bar{\psi}\gamma^\mu\psi)$ , and isovector-vector  $(\bar{\psi}\vec{\tau}\gamma_\mu\psi) \cdot (\bar{\psi}\vec{\tau}\gamma^\mu\psi)$ . The Lagrangian of the PC-RMF model contains four-fermion (contact) interaction terms:

$$\begin{aligned}
 \mathcal{L} = & \bar{\psi}(i\gamma \cdot \partial - m)\psi \\
 & - \frac{1}{2}\alpha_s(\hat{\rho}_v)(\bar{\psi}\psi)(\bar{\psi}\psi) - \frac{1}{2}\alpha_v(\hat{\rho}_v)(\bar{\psi}\gamma^\mu\psi)(\bar{\psi}\gamma_\mu\psi) \\
 & - \frac{1}{2}\alpha_{tv}(\hat{\rho}_v)(\bar{\psi}\vec{\tau}\gamma^\mu\psi)(\bar{\psi}\vec{\tau}\gamma_\mu\psi) \\
 & - \frac{1}{2}\delta_s(\partial_\nu\bar{\psi}\psi)(\partial^\nu\bar{\psi}\psi) - e\bar{\psi}\gamma \cdot A\frac{(1-\tau_3)}{2}\psi. \tag{11}
 \end{aligned}$$

The last term therein defines the coupling of the protons to the electromagnetic four-potential. The derivative term in Eq. (11) accounts for next-order effects from a density-matrix expansion of finite-range and correlation effects [21, 22]. Although one could include a derivative term in each spin-isospin channel, in practice ground-state data can constrain only a single derivative term. In particular, DD-PC1 implements this term in the isoscalar-scalar channel. The strength parameters  $\alpha_c$  of the interaction terms in Eq. (11) are density-dependent functionals of  $\sqrt{j^\mu j_\mu}$ , with the nucleon 4-current:  $j^\mu = \bar{\psi}\gamma^\mu\psi$ . However, at low velocities relevant for the present investigation, the parameters  $\alpha_c$  depend only on the baryon density  $\hat{\rho}_v = \psi^\dagger\psi$ . The single-nucleon Dirac equation, that is, the relativistic analogue of the Kohn-Sham equation [23], is obtained from the variation of the Lagrangian with respect to  $\bar{\psi}$ . This yields:

$$[\gamma_\mu(i\partial^\mu - \Sigma^\mu - \Sigma_R^\mu) - (m + \Sigma_S)]\psi = 0, \tag{12}$$

with the nucleon self-energies  $\Sigma$  defined by the following relations:

$$\Sigma^\mu = \alpha_V(\rho_v)j^\mu + e\frac{(1-\tau_3)}{2}A^\mu \tag{13}$$

$$\Sigma_R^\mu = \frac{1}{2}\frac{j^\mu}{\rho_v} \left\{ \frac{\partial\alpha_s}{\partial\rho}\rho_s^2 + \frac{\partial\alpha_v}{\partial\rho}j_\mu j^\mu + \frac{\partial\alpha_{tv}}{\partial\rho}\vec{j}_\mu \vec{j}^\mu \right\} \tag{14}$$

$$\Sigma_S = \alpha_s(\rho_v)\rho_s - \delta_s\Box\rho_s \tag{15}$$

$$\Sigma_{TV}^\mu = \alpha_{tv}(\rho_v)\vec{j}^\mu. \tag{16}$$

In addition to contributions from the isoscalar-vector four-fermion interaction and the electromagnetic interaction, the isoscalar-vector self-energy includes the ‘‘rearrangement’’ terms  $\Sigma_R^\mu$  that arise from the variation of the vertex functionals  $\alpha_s$ ,  $\alpha_v$ , and  $\alpha_{tv}$  with respect to the nucleon fields in the vector density operator  $\hat{\rho}_v$ . The importance of self-energies  $\Sigma$  becomes more apparent in the non-relativistic limit [7]. Of particular interest is the interplay between the scalar  $\Sigma_S$  and the vector component  $\Sigma^0$ . The non-relativistic local mean-field potential is determined by the sum  $\Sigma_S + \Sigma^0$ , which is relatively small because these self-energies have opposite signs. The difference  $\Sigma_S - \Sigma^0$ , on the other hand, is large and explains the comparatively large energy spacings between spin-orbit partner states [24]. Thus the sum and difference of the isoscalar-scalar and isoscalar-vector self-energies relate to very different physical effects.

At the mean-field level the nuclear ground state  $|\phi_0\rangle$  is represented by the self-consistent solution of the system of equations (12) – (16), with the ground-state isoscalar

and isovector four-currents and scalar density defined as expectation values:

$$j_\mu = \langle \phi_0 | \bar{\psi} \gamma_\mu \psi | \phi_0 \rangle = \sum_{k=1}^N v_k^2 \bar{\psi}_k \gamma_\mu \psi_k , \quad (17)$$

$$\vec{j}_\mu = \langle \phi_0 | \bar{\psi} \gamma_\mu \vec{\tau} \psi | \phi_0 \rangle = \sum_{k=1}^N v_k^2 \bar{\psi}_k \gamma_\mu \vec{\tau} \psi_k , \quad (18)$$

$$\rho_s = \langle \phi_0 | \bar{\psi} \psi | \phi_0 \rangle = \sum_{k=1}^N v_k^2 \bar{\psi}_k \psi_k , \quad (19)$$

where  $\psi_k$  are Dirac spinors, and the sum runs over occupied positive-energy single-nucleon orbitals, including the corresponding occupation factors  $v_k^2$ . The single-nucleon Dirac equations are solved self-consistently in the “*no-sea*” approximation, that omits explicit contributions of negative-energy solutions of the relativistic equations to densities and currents [4, 7, 8].

In a phenomenological construction of a relativistic energy density functional one starts from an assumed ansatz for the medium dependence of the mean-field nucleon self-energies, and adjusts the free parameters directly to ground-state data on finite nuclei. Guided by the microscopic density dependence of the vector and scalar self-energies, the following practical ansatz for the functional form of the couplings was adopted in Ref. [2]:

$$\begin{aligned} \alpha_s(\rho) &= a_s + (b_s + c_s x) e^{-d_s x} , \\ \alpha_v(\rho) &= a_v + b_v e^{-d_v x} , \\ \alpha_{tv}(\rho) &= b_{tv} e^{-d_{tv} x} , \end{aligned} \quad (20)$$

with  $x = \rho/\rho_{\text{sat}}$ , where  $\rho_{\text{sat}}$  denotes the nucleon density at saturation in symmetric nuclear matter. The set of 10 strength parameters was adjusted in a multistep parameter fit exclusively to the experimental masses of 64 axially deformed nuclei in the mass regions  $A \approx 150 - 180$  and  $A \approx 230 - 250$ . The resulting functional DD-PC1 [2] has been further tested in calculations of binding energies, charge radii, deformation parameters, neutron skin thickness, and excitation energies of giant monopole and dipole resonances. The parameters of DD-PC1 are given in Table 1. The nuclear matter equation of state that corresponds to DD-PC1 is characterized by the following properties at the saturation point: nucleon density  $\rho_{\text{sat}} = 0.152 \text{ fm}^{-3}$ , volume energy  $a_v = -16.06 \text{ MeV}$ , surface energy  $a_s = 17.498 \text{ MeV}$ , symmetry energy  $a_4 = 33 \text{ MeV}$ , and the nuclear matter compression modulus  $K_{nm} = 230 \text{ MeV}$  (see also table 2).

Although we could analyze correlations between the individual parameters  $a_i$ ,  $b_i$ ,  $c_i$  and  $d_i$  in Eq. (20), we choose to examine correlations between the lowest-order terms in a Taylor expansion of the density-dependent coupling functions around the saturation point:  $\alpha_i(\rho_{\text{sat}})$ ,  $\alpha'_i(\rho_{\text{sat}})$  and  $\alpha''_i(\rho_{\text{sat}})$ , because these quantities directly determine the expressions for the binding energy, pressure and compressibility of nuclear matter at saturation. Also, such an analysis could lead to more general conclusions that can be related to other density functionals, rather than just the one defined by the couplings in

**Table 1.** Parameters of the relativistic energy density functional DD-PC1 (cf. Eq. (20)). The value of the nucleon mass is  $m = 939$  MeV.

PARAMETER	
$a_s$ (fm <sup>2</sup> )	-10.0462
$b_s$ (fm <sup>2</sup> )	-9.1504
$c_s$ (fm <sup>2</sup> )	-6.4273
$d_s$	1.3724
$a_v$ (fm <sup>2</sup> )	5.9195
$b_v$ (fm <sup>2</sup> )	8.8637
$d_v$	0.6584
$b_{tv}$ (fm <sup>2</sup> )	1.8360
$d_{tv}$	0.6403
$\delta_s$ (fm <sup>4</sup> )	-0.8149

Eq. (20). For the isovector channel, we will use the values of the parameters  $\alpha_{tv}(\rho_{\text{sub}})$  and  $\alpha'_{tv}(\rho_{\text{sub}})$  at the sub-saturation density of  $\rho_{\text{sub}} = 0.12 \text{ fm}^{-3}$ .

For the isoscalar-scalar channel we hold on to the parameter  $d_s$ , and express  $a_s$ ,  $b_s$  and  $c_s$  in terms of the coupling  $\alpha_s(\rho_{\text{sat}})$  and the corresponding derivatives

$$c_s = -\frac{\rho_{\text{sat}}}{d_s} e^{d_s} [d_s \alpha'_s(\rho_{\text{sat}}) + \rho_{\text{sat}} \alpha''_s(\rho_{\text{sat}})], \quad (21)$$

$$b_s = c_s \left( \frac{1}{d_s} - 1 \right) - \alpha'_s(\rho_{\text{sat}}) \rho_{\text{sat}} \frac{e^{d_s}}{d_s}, \quad (22)$$

$$a_s = \alpha_s(\rho_{\text{sat}}) - (b_s + c_s) e^{-d_s}. \quad (23)$$

In the isoscalar-vector term there are only three parameters  $a_v$ ,  $b_v$  and  $d_v$ , which can be expressed as

$$d_v = -\frac{\alpha''_v(\rho_{\text{sat}})}{\alpha'_v(\rho_{\text{sat}})} \rho_{\text{sat}}, \quad (24)$$

$$b_v = -\alpha'_v(\rho_{\text{sat}}) \frac{e^{d_v}}{d_v}, \quad (25)$$

$$a_v = \alpha_v(\rho_{\text{sat}}) - b_v e^{-d_v}. \quad (26)$$

Finally, the isovector-vector channel of the functional DD-PC1 is determined by two parameters only. These are expressed through the values of the coupling  $\alpha_{tv}$  and its derivative  $\alpha'_{tv}$  at sub-saturation density  $\rho_{\text{sub}} = 0.12 \text{ fm}^{-3}$ :

$$d_{tv} = -\rho_{\text{sat}} \frac{\alpha'_{tv}(\rho_{\text{sub}})}{\alpha_{tv}(\rho_{\text{sub}})}, \quad (27)$$

$$b_{tv} = \alpha_{tv}(\rho_{\text{sub}}) e^{d_{tv}(\rho_{\text{sub}}/\rho_{\text{sat}})}. \quad (28)$$

#### 4. Infinite and semi-infinite nuclear matter

The parameters of the functional DD-PC1 given in Table 1, or the corresponding terms in the Taylor expansion of the density-dependent couplings around the saturation point defined in the previous section, correspond to the “best model”, that is, they determine the point  $\mathbf{p}_0$  in the  $F$ -dimensional parameter space. In this section we would like to study the “uniqueness” of DD-PC1, defined in the sense of Ref. [16]. For this we start with the basic system for which an energy density functional can give definite predictions, that is, infinite nuclear matter. In this system we define a set of  $N$  pseudo-observables ( $N > F$ ) that can be used to compute the quality measure  $\chi^2(\mathbf{p})$ . The model is “unique” if all the eigenvalues of the  $F \times F$  matrix of second derivatives  $\mathcal{M}$  in Eq. (5) are large, that is, if all the eigenvectors correspond to stiff directions in the parameter space along which the function  $\chi^2$  increases rapidly and, therefore, the corresponding linear combinations of parameters are tightly constrained by the selected observables.

**Table 2.** Pseudo-observables for infinite nuclear matter used to compute the quality measure  $\chi^2$ -function of DD-PC1. The binding energy is evaluated at three density points: the saturation density  $\rho_0$ , at lower density  $\rho_{low} = 0.04 \text{ fm}^{-3}$ , and higher density  $\rho_{high} = 0.56 \text{ fm}^{-3}$ . The compressibility modulus  $K_0$ , the Dirac mass  $m_D$ , the effective mass  $m^*$ , and the symmetry energy coefficient  $a_4$ , correspond to the saturation density. The values of the symmetry energy  $S_2$  and its slope  $L$  are given at the sub-saturation density  $\rho_{sub} = 0.12 \text{ fm}^{-3}$ , which is relevant when calculating binding energies and collective excitations of finite nuclei.

OBSERVABLE	DD-PC1
$\rho_0$	$0.152 \text{ fm}^{-3}$
$\epsilon(\rho_0)$	-16.06 MeV
$\epsilon(\rho_{low})$	-6.48 MeV
$\epsilon(\rho_{high})$	34.38 MeV
$K_0$	230 MeV
$m_D$	0.58
$m^*$	0.66
$S_2(\rho_{sub})$	27.8 MeV
$L(\rho_{sub})$	57.2 MeV
$a_4$	33 MeV

Table 2 lists the values of ten pseudo-observables for infinite nuclear matter generated with the functional DD-PC1. In addition to the quantities that are evaluated at the saturation point (nucleon density  $\rho_{sat} = 0.152 \text{ fm}^{-3}$ , volume energy  $a_v = -16.06 \text{ MeV}$ , symmetry energy  $a_4 = 33 \text{ MeV}$ , the Dirac mass  $m_D = m + \alpha_s \rho_s = 0.58m$ , the non-relativistic effective mass [25, 26]  $m^* = m - \alpha_v \rho_v = 0.66 m$ , and the nuclear matter compression modulus  $K_{nm} = 230 \text{ MeV}$ ), we have included four more quantities that characterise the equation of state of symmetric and asymmetric matter at lower

and higher densities: the binding energy of symmetric nuclear matter at low density  $\rho_{low} = 0.04 \text{ fm}^{-3}$  and high density  $\rho_{high} = 0.56 \text{ fm}^{-3}$ ; and both the symmetry energy  $S_2$  and its slope  $L$  at the sub-saturation density  $\rho_{sub} = 0.12 \text{ fm}^{-3}$ . The isoscalar derivative term in Eq. (11) does not contribute in the case of infinite homogeneous nuclear matter, and thus the surface energy is not included in the set of ten pseudo-observables. Since we are considering quantities that cannot be directly measured, to calculate the quality function  $\chi^2$  and the matrix of second derivatives at the point  $\mathbf{p}_0$  (DD-PC1) an arbitrary uncertainty of 2% is assigned to each observable. We are, of course, aware that the empirical values of some of the ten pseudo-observables are constrained better than others, e.g. binding energy or compressibility, as compared to the slope of symmetry energy. However, this is not crucial for the present consideration and thus we prefer to assign the same uncertainty to each observable in Table 2.

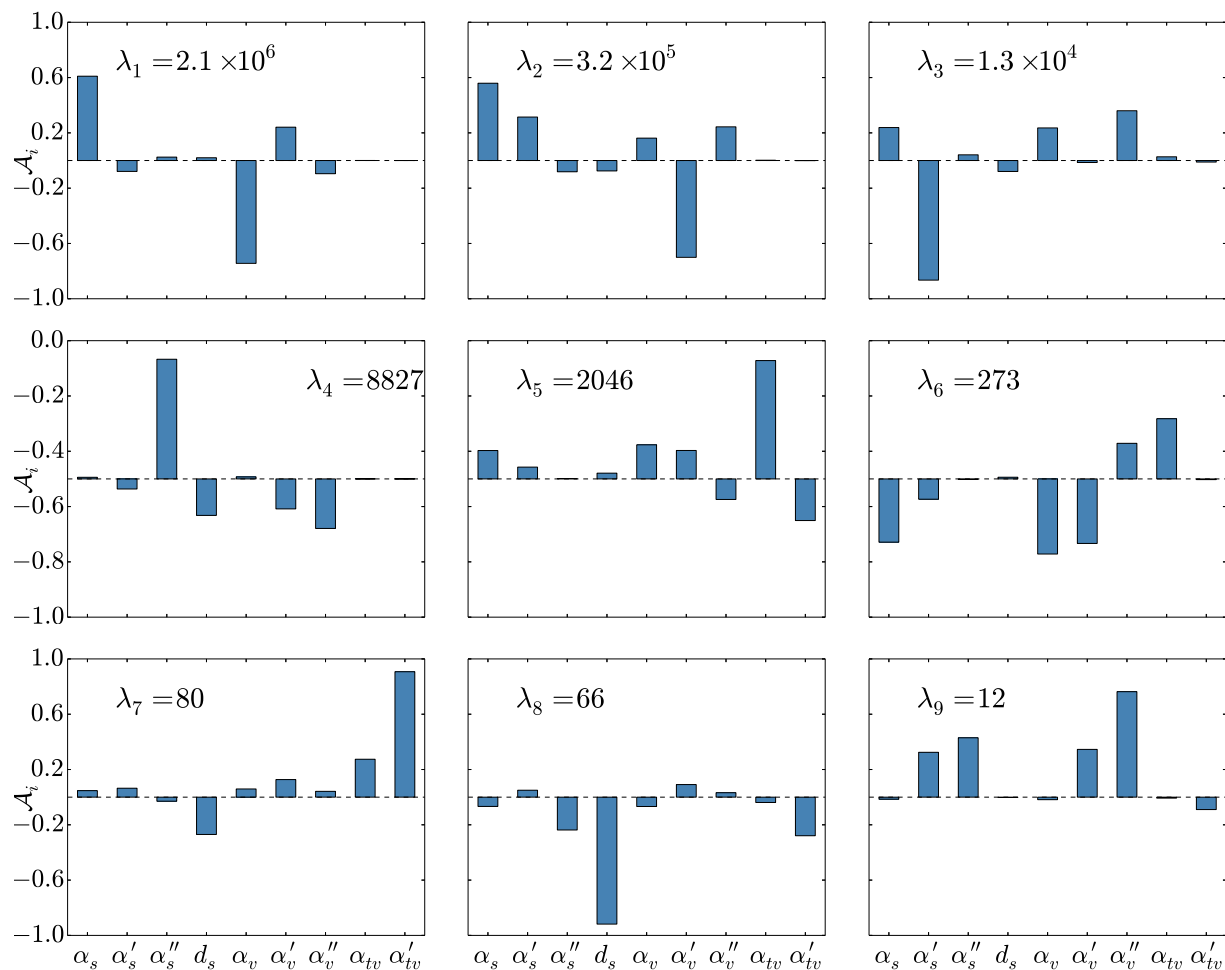


**Figure 1.** (Color online) Eigenvalues and eigenvectors of the  $9 \times 9$  matrix of second derivatives  $\mathcal{M}$  of  $\chi^2(\mathbf{p})$  in symmetric nuclear matter for the functional DD-PC1.

The symmetric  $9 \times 9$  matrix  $\mathcal{M}$  of second derivatives of  $\chi^2(\mathbf{p})$  at the point  $\mathbf{p}_0$  (DD-PC1) is diagonalized by means of an orthogonal transformation. The diagonal

matrix elements in order of decreasing values and the components of the corresponding eigenvectors are displayed in Fig. 1. Stiff directions in the nine-parameter space are characterised by large eigenvalues, that is, the function  $\chi^2$  increases rapidly along these directions. This means that the particular linear combinations of parameters corresponding to the stiff eigenvectors are firmly determined by the pseudo-data listed in Table 2. On the other hand, comparatively small eigenvalues belong to soft directions in the multi-parameter space, along which the quality measure displays little deterioration and the corresponding linear combinations of parameters that define the energy density functional are poorly constrained.

The four stiffest directions in Fig. 1 are dominated by isoscalar parameters, as denoted by the components of the corresponding eigenvectors, whereas the fifth, sixth and seventh eigenvector contain sizeable admixtures of isovector parameters. The two softest directions are again predominantly isoscalar. The first mode, characterised by the largest eigenvalue, corresponds to out-of-phase oscillations of the  $\alpha_s(\rho_{\text{sat}})$  and  $\alpha_v(\rho_{\text{sat}})$  coupling parameters. This combination of parameters is tightly constrained by the three values of the nuclear matter binding energy. An increase of the scalar attraction and a simultaneous decrease of the vector repulsion leads to a pronounced increase of the binding energy, as described in the previous section and, therefore, to a rapid deterioration of  $\chi^2$ . Mode two, which corresponds to out-of-phase oscillations of the derivatives  $\alpha'_s(\rho_{\text{sat}})$  and  $\alpha'_v(\rho_{\text{sat}})$ , is predominantly constrained by the values of the binding energy at  $\rho_{\text{low}}$  and  $\rho_{\text{high}}$  because the slope of the couplings at saturation density determines the values of the corresponding couplings below and above the saturation density. Mode three is mostly determined by the saturation density, whereas for mode four the largest amplitudes correspond to components that represent the second derivatives of isoscalar couplings, that is, this mode is constrained by the nuclear matter incompressibility.

Modes number five and six correspond to superpositions of the isoscalar and isovector modes, and are constrained by the value of  $S_2$  and the Dirac mass, which enters into the expression for the symmetry energy

$$S_2(\rho) = \frac{k_f^2}{6\sqrt{k_f^2 + m_D^2}} + \frac{1}{2}\alpha_{tv}(\rho)\rho. \quad (29)$$

Because we consider the value of the symmetry energy at sub-saturation density, both the couplings and their derivatives ( $\alpha_s(\rho_{\text{sat}})$ ,  $\alpha'_s(\rho_{\text{sat}})$ ,  $\alpha_v(\rho_{\text{sat}})$ ,  $\alpha'_v(\rho_{\text{sat}})$ ) contribute to these modes. When the slope of the symmetry energy is calculated, both the coupling  $\alpha_{tv}(\rho)$  and its derivative  $\alpha'_{tv}(\rho)$  contribute, as signaled by the in-phase isovector components in mode seven.

Mode number eight corresponds almost entirely to the parameter  $d_s$  in the isoscalar-scalar channel (cf. Eq. (20)), which is obviously poorly determined by the pseudo-data in Tab. 2. The softest mode represents the in-phase contributions from the first and second derivatives of the isoscalar couplings at saturation density.

The uncertainties, that is, the variances of model parameters are given by the

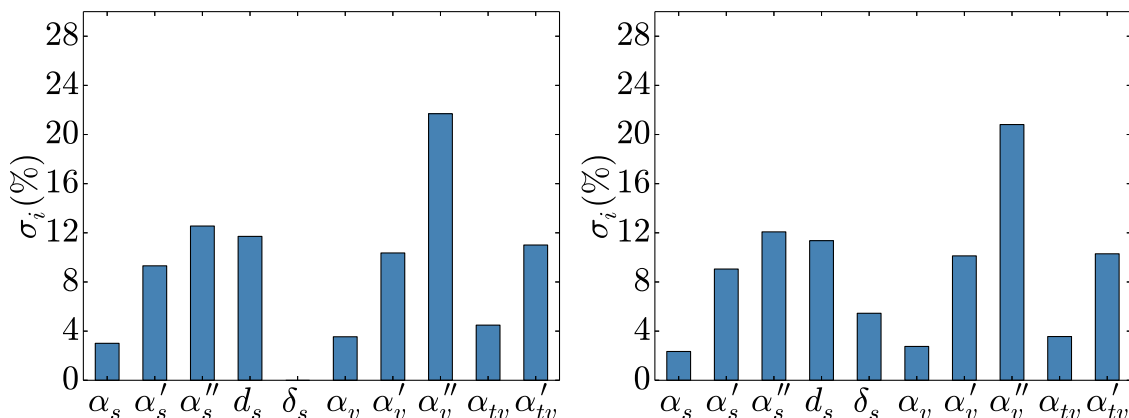


**Figure 2.** (Color online) Uncertainties  $\sigma_i$  in percentage of the model parameters for the functional DD-PC1. Results displayed in the left panel correspond to a calculation with pseudo-observables of infinite nuclear matter, while those in the right panel have been obtained by including also the surface energy of semi-infinite nuclear matter.

diagonal elements of the inverse matrix  $\mathcal{M}^{-1}$  of second derivatives of  $\chi^2$  – the covariance matrix (cf. Eq. (7))

$$\sigma_i^2 = (\mathcal{M}^{-1})_{ii} = (\mathcal{A}\mathcal{D}^{-1}\mathcal{A}^T)_{ii} = \sum_{j=1}^9 \mathcal{A}_{ij}\lambda_j^{-1}. \quad (30)$$

For each parameter  $p_i = p_{0i}(1 \pm \sigma_i)$ , the uncertainty  $\sigma_i$  in percentage is shown in the left panel of Fig. 2. As one would have expected, the values of the couplings  $\alpha_s(\rho_{\text{sat}})$ ,  $\alpha_v(\rho_{\text{sat}})$  and  $\alpha_{tv}(\rho_{\text{sub}})$  have the smallest uncertainties ( $\leq 5\%$ ), whereas uncertainties increase rapidly for their first and second derivatives. This result already indicates that a particular choice for the density dependence of coupling functions can lead to large model uncertainties. As shown in Fig. 1, the parameter  $d_s$  completely determines the very soft mode number eight, and the corresponding uncertainty of this parameter is rather large ( $> 10\%$ ). The uncertainty of  $\delta_s$  is zero because the corresponding term does not contribute to homogeneous nuclear matter.

The correlation coefficients between model parameters are determined by the off-diagonal elements of the covariance matrix:

$$\rho(p_i, p_j) = \frac{\mathcal{M}_{ij}^{-1}}{\sqrt{\mathcal{M}_{ii}^{-1}\mathcal{M}_{jj}^{-1}}}. \quad (31)$$

The color coded plot of the 36 independent correlation coefficients for the present calculation of infinite nuclear matter is displayed in the left panel of Fig. 3. One notices the strong correlations between the isoscalar scalar and isoscalar vector couplings, as well as between their first derivatives and also second derivatives. There is also a significant correlation between  $\alpha_{tv}(\rho_{\text{sub}})$  and  $\alpha'_{tv}(\rho_{\text{sub}})$  because the coupling  $\alpha_{tv}(\rho_{\text{sub}})$  enters the expression for the slope of the symmetry energy. The correlation between the isoscalar

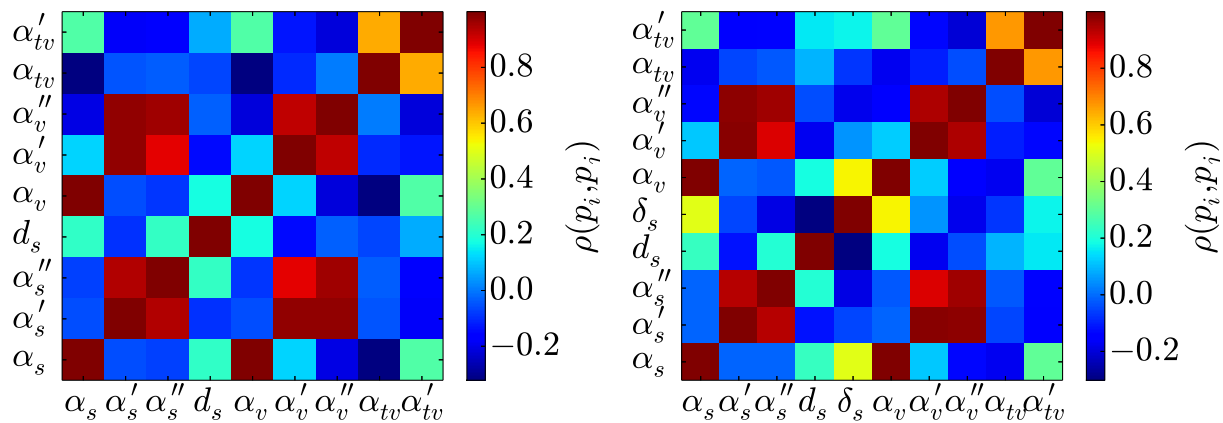


**Figure 3.** (Color online) Left: color-coded plot of the 36 independent correlation coefficients between the 9 model parameters that contribute to the calculation for infinite nuclear matter. Right: color-coded plot of the 45 independent correlation coefficients between the 10 model parameters that contribute when semi-infinite nuclear matter is included in the calculation.

and isovector parameters originates from the Dirac mass contribution to the symmetry energy.

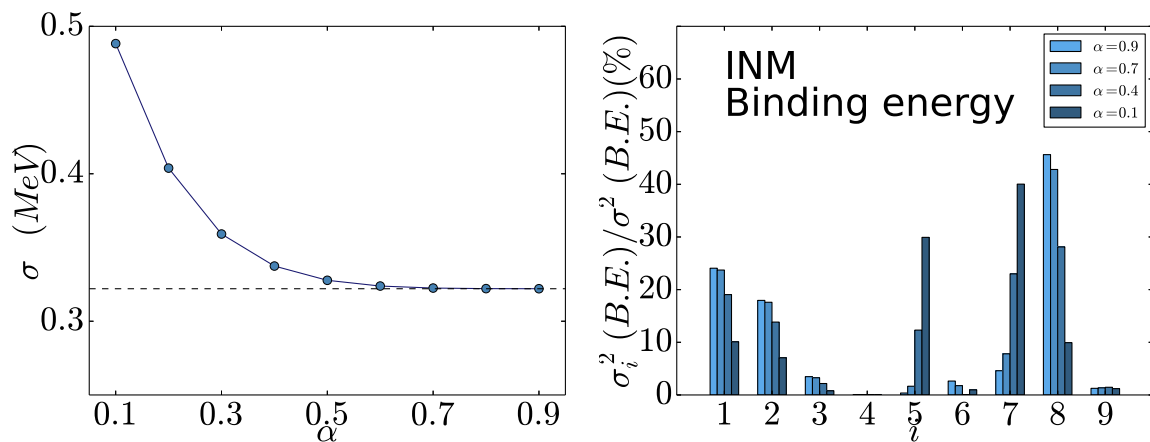


**Figure 4.** (Color online) Left: calculated uncertainty of the binding energy of asymmetric nuclear matter at the saturation density  $\rho_0 = 0.152 \text{ fm}^{-3}$ , as a function of the asymmetry parameter. Right: relative contributions in percentage of the nine linear combinations of model parameters that correspond to the eigenvectors of the matrix of second derivatives  $\mathcal{M}$  in Eq. (5) to the variance of the binding energy of asymmetric nuclear matter.

In the left panel of Fig. 4 we plot the calculated uncertainty  $\sigma(\epsilon(\rho_0)) = \sqrt{\text{var}(\epsilon(\rho_0))}$  of the binding energy of asymmetric nuclear matter at the saturation density  $\rho_0 = 0.152 \text{ fm}^{-3}$ , as a function of the asymmetry parameter. The asymmetry parameter  $\alpha$  is defined

by the relation

$$\alpha = \frac{\rho_p}{\rho_n} \implies \rho_n = \frac{\rho}{1 + \alpha}, \quad \rho_p = \rho - \rho_n = \frac{\alpha\rho}{1 + \alpha}. \quad (32)$$

For symmetric nuclear matter the asymmetry parameter equals one, and it goes to zero for pure neutron matter. The dashed horizontal line corresponds to the assumed 2% uncertainty in symmetric nuclear matter. The calculated uncertainty exhibits a rapid increase when nuclear matter becomes neutron rich and, in finite nuclei, this would result in a corresponding increase of the standard error of calculated binding energies for systems with a large neutron excess, as shown in the analysis of the propagation of uncertainties in Skyrme energy density functionals [20]. For four values of  $\alpha$ , the right panel of Fig. 4 displays the individual relative contributions from each of the nine linear combinations of model parameters, that correspond to the eigenvectors of the matrix of second derivatives  $\mathcal{M}$  in Eq. (5), to the variance of the binding energy of asymmetric nuclear matter. Here one can clearly identify the source of the increase in uncertainty  $\sigma(\epsilon(\rho_0))$  with decreasing  $\alpha$ . As the neutron excess increases, we notice a pronounced increase in the relative contributions of the eigenvectors (modes) five and seven (see Fig. 1) to the variance of the binding energy. These two modes are dominated by the two isovector parameters: the values of the coupling  $\alpha_{tv}$  and its derivative  $\alpha'_{tv}$  at sub-saturation density, respectively. The uncertainties of the isovector parameters, especially of the slope of the symmetry energy, determine the pronounced increase of the uncertainty of the binding energy in asymmetric nuclear matter.

To analyze the uncertainty and the corresponding correlations for the strength parameter  $\delta_s$  of the derivative term in Eq. (11), we have extended the calculation of the quality measure  $\chi^2(\mathbf{p})$  and the corresponding matrix of second derivatives  $\mathcal{M}$  in Eq. (5) to include semi-infinite nuclear matter. For the surface energy we take the empirical value  $a_s = 17.5$  MeV with a 2% uncertainty, the same as for the other pseudo-data. The dimension of the matrix  $\mathcal{M}$  of second derivatives is now  $10 \times 10$ , and the diagonal matrix elements in order of decreasing values and the components of the corresponding eigenvectors are displayed in Fig. 5. The distribution of components for most of the modes is very similar to those already shown in Fig. 1, and we note that only the sixth and seventh eigenvectors contain significant amplitudes that arise from the derivative term. These eigenvectors also contain in-phase contributions from the isoscalar scalar and vector couplings, signaling that they are to some extent constrained by the effective mass. Because of the contribution of the effective mass to the symmetry energy, modes number six and seven contain sizeable amplitudes from the isovector channel.

The theoretical uncertainties and correlation coefficients for the model parameters, shown in the panels on the right of Fig. 2 and Fig. 3, respectively, are not significantly altered by the inclusion of the surface energy of semi-infinite nuclear matter in the set of pseudo-observables. We note, however, that the uncertainty of the parameter  $\delta_s$  of the derivative term is larger than those of  $\alpha_s(\rho_{\text{sat}})$  and  $\alpha_v(\rho_{\text{sat}})$ , with which  $\delta_s$  displays significant correlation.

Finally, in Fig. 6 we plot the relative contributions from the ten eigenvectors of the

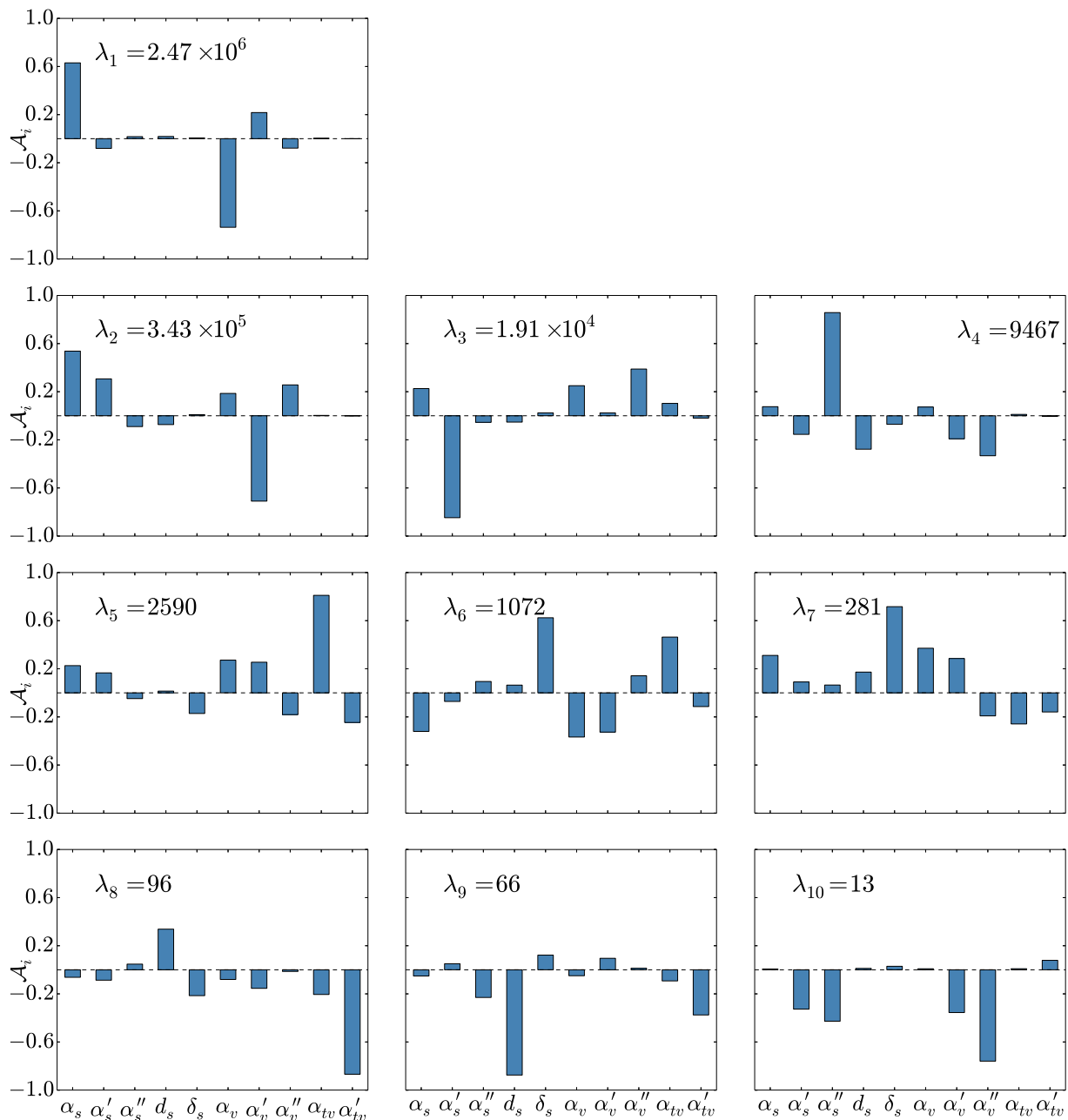


**Figure 5.** (Color online) Same as in the caption to Fig. 1, but now the model parameter space includes the strength  $\delta_s$  of the derivative term in Eq. (11), and the surface energy of semi-infinite nuclear matter is added to the set of pseudo-data used to calculate  $\chi^2$ .

matrix  $\mathcal{M}$  to the variance of the surface energy and surface thickness of semi-infinite nuclear matter (SINM). The largest contribution to the variance of the surface energy corresponds to mode six, which is dominated by the strength parameter of the isoscalar derivative term. The variance of the surface thickness, which has not been included in the set of pseudo-data used to calculate  $\chi^2(\mathbf{p})$ , displays an even more pronounced contribution from mode nine which predominantly corresponds to the parameter  $d_s$  of

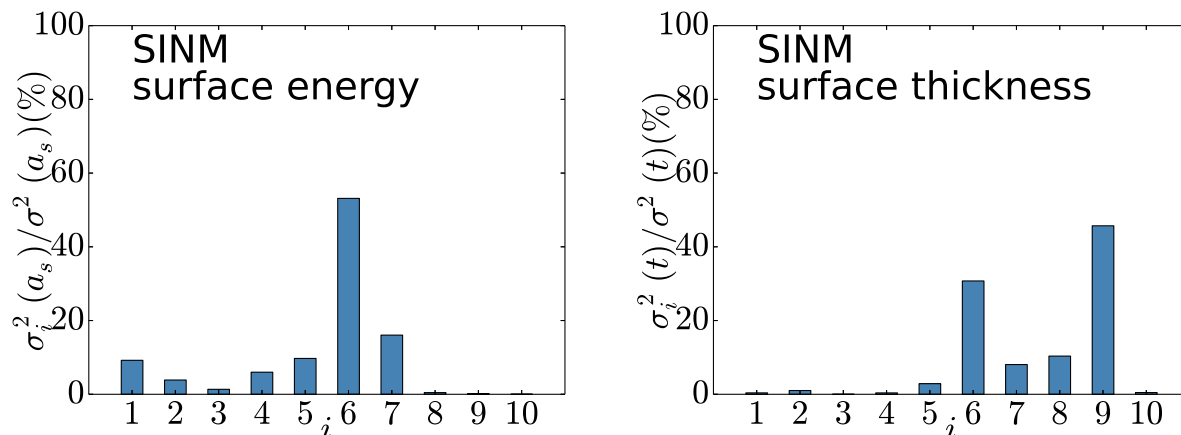


**Figure 6.** (Color online) Relative contributions in percentage of the ten linear combinations of model parameters that correspond to the eigenvectors of the matrix of second derivatives  $\mathcal{M}$  in Eq. (5) (see Fig. 5), to the variances of the surface energy and surface thickness of semi-infinite nuclear matter .

the isoscalar scalar coupling (cf. Eq. (20)).

## 5. Finite nuclei

In this section we extend the calculation of variances to ground-state observables of finite nuclei: binding energies and charge radii. Ground-state properties of spherical and deformed nuclei are computed in the framework of the relativistic Hartree-Bogoliubov model [9]. In addition to the energy density functional in the particle-hole channel, pairing correlations are taken into account by using an interaction that is separable in momentum space, and determined by two parameters adjusted to reproduce the empirical pairing gap in symmetric nuclear matter. As already explained in Sec. 3, the 10 parameters of the functional DD-PC1 were determined by a fit to the experimental masses of 64 axially deformed nuclei in the mass regions  $A \approx 150-180$  and  $A \approx 230-250$  [2]. In a series of subsequent studies it has been shown that this functional provides accurate predictions for binding energies, charge radii, deformation parameters, neutron skin thickness, and excitation energies of giant monopole and dipole resonances, as well as spectroscopic properties calculated using the generator coordinate method and/or the generalized quadrupole collective Hamiltonian [27]. In Figs. 7 and 8 we display the relative contributions of the ten linear combinations of model parameters that correspond to the eigenvectors of the matrix of second derivatives  $\mathcal{M}$  to the variances of the binding energy for a representative set of rare-earth and actinide nuclei, respectively. In both mass regions the largest contribution to the variance of the binding energy originates from the next-to-softest mode number nine, dominated by the parameter  $d_s$  in the isoscalar-scalar channel (cf. Eq. (20)). Modes number one and two correspond to out-of-phase contributions of the isoscalar couplings and their first derivatives at saturation density, respectively, and correspond to stiff directions in the parameter

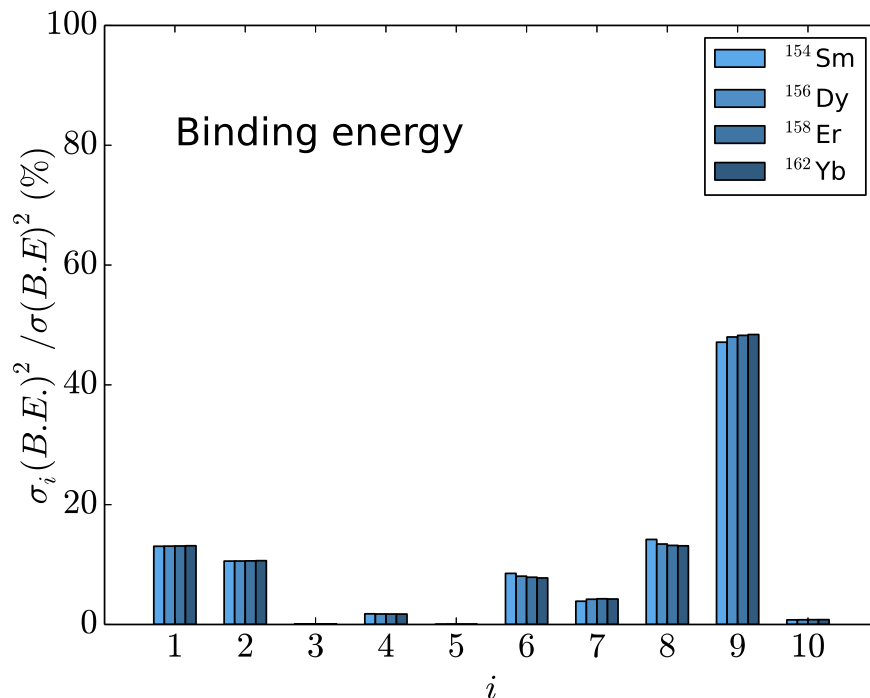


**Figure 7.** (Color online) Relative contributions in percentage of the ten linear combinations of model parameters that correspond to the eigenvectors of the matrix of second derivatives  $\mathcal{M}$  Eq. (5) (see Fig. 5), to the variances of the binding energy of rare-earth nuclei.

space. Finally, more pronounced contributions to the variance of the binding energy result also from the soft modes number six and eight, which correspond to combinations of isoscalar and isovector parameters: predominantly  $\delta_s$  and  $\alpha_{tv}$  in mode six, and  $d_s$  and the derivative  $\alpha'_{tv}$  in mode eight.

In contrast to rare-earth nuclei and actinides, spherically symmetric nuclei and, in particular, tin isotopes were not included in the adjustment of the parameters of DD-PC1. Nevertheless, one finds essentially the same distribution of eigenvectors of the matrix of second derivatives of  $\chi^2(\mathbf{p})$  in the variance of binding energies of tin isotopes. This is shown in the upper panel of Fig. 9, where we plot the relative contributions of the eigenmodes of  $\mathcal{M}$  to the variance of the binding energies of Sn nuclei with mass number  $100 \leq A \leq 148$ . The fact that the largest contribution to the variances originates from the next-to-softest mode, that is, from a combination of parameters ( $d_s$  and the derivative  $\alpha'_{tv}$ ) poorly constrained by the set of pseudo-data that determine  $\chi^2(\mathbf{p})$ , indicates that the choice for the ansatz of the density dependence of the isoscalar-scalar coupling (cf. Eq. (20)) should be reexamined. We also note the increase of the relative contribution of the, predominantly isovector, mode eight in tin isotopes with a larger neutron excess. It is particularly interesting to compare the relative contributions to the variance of the binding energy to those of an observable that was not included in the fit of the parameters of DD-PC1. The lower panel of Fig. 9 displays the relative contributions

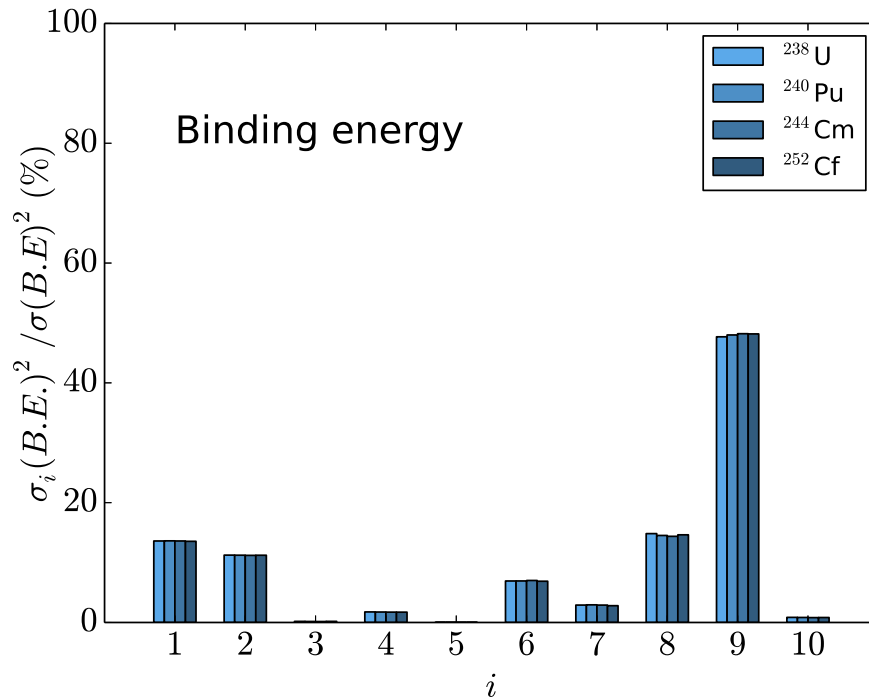


**Figure 8.** (Color online) Same as in the caption to Fig. 7 but for the binding energy of actinide nuclei.

of the eigenmodes of  $\mathcal{M}$  to the variance of the radius of the proton distribution of tin isotopes. In this case the variance for all isotopes is dominated by the relatively stiff combination of parameters that corresponds to mode three, and its relative contribution increases with neutron number. The significant contributions from the soft modes six, seven, and eight decrease in neutron-rich tin isotopes whereas, as one would expect, the out-of-phase contributions of isoscalar couplings in the stiff mode one do not show significant variation with neutron number.

## 6. Conclusion

Nuclear density functional theory (NDFT) provides a unified framework for studies of ground-state properties and collective excitations across the nuclide chart. Even though methods and structure models based on DFT have been extremely successful in analyzing a variety of nuclear properties and predicting new structure phenomena, a fully microscopic foundation of nuclear energy density functionals (NEDFs), based on and constrained by the underlying theory of strong interactions, has yet to be established. However, even if this task is accomplished in future, the parameters of a NEDF will have to be fine-tuned to data on finite, medium-heavy and heavy nuclei. This is because of the inherent complexity of the effective in-medium inter-nucleon interactions that cannot fully be unfolded starting from the fundamental low-energy degrees of freedom, nor by data on nucleon-nucleon scattering and few-nucleon systems.

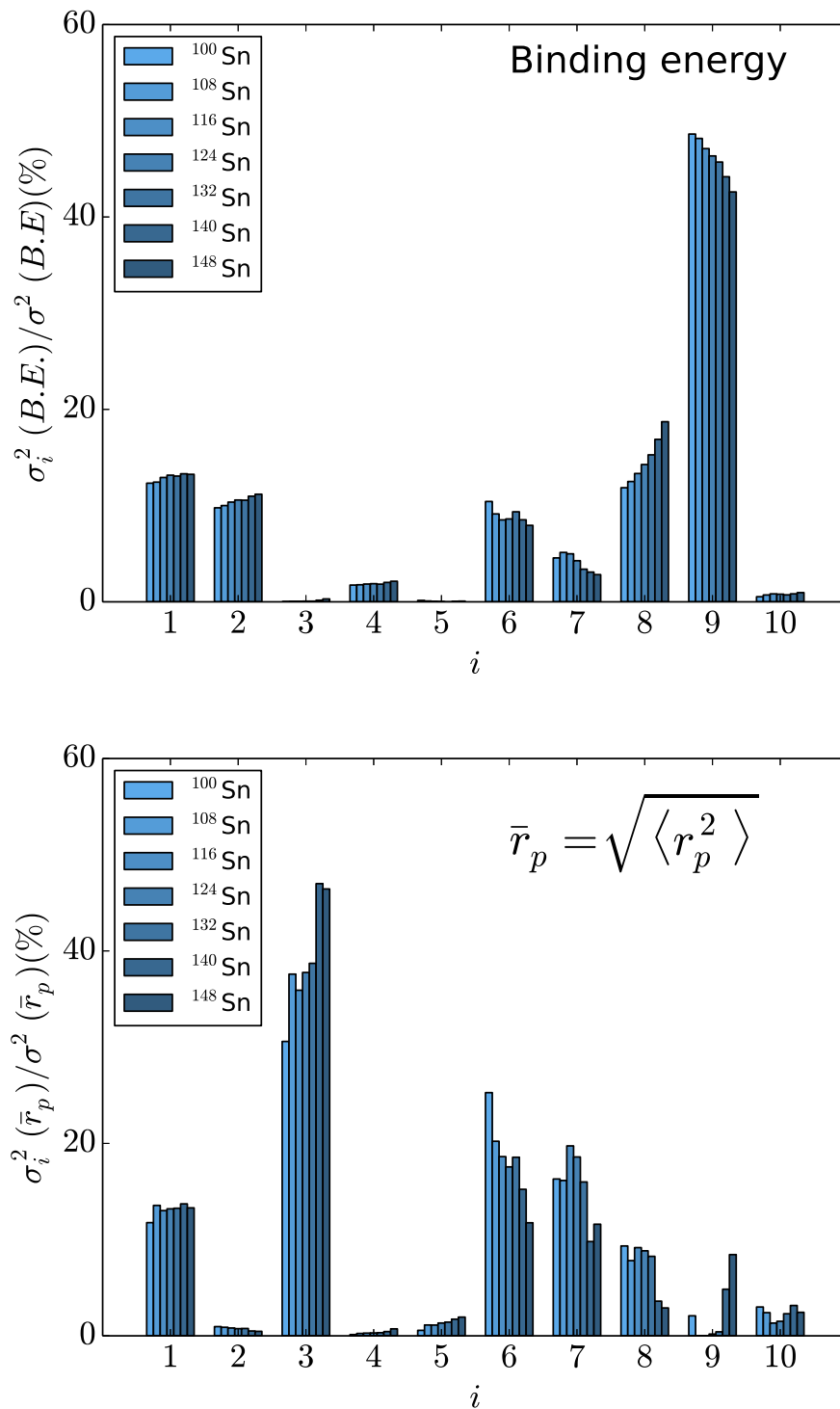


**Figure 9.** (Color online) Same as in the caption to Fig. 7 but for the binding energies (upper panel), and radii of the proton distribution (lower panel) of tin isotopes.

Some of the most successful NEDFs are semi-phenomenological and approximate the exact unknown functional by an expansion in powers of ground-state nucleon

densities and currents and their gradients, and/or assume a relatively simple ansatz for the density dependence of the effective inter-nucleon interactions, often based on a microscopic nuclear matter equation of state. The problem then becomes how to select the most efficient functional form and/or parametrization of the density dependence, considering the fact that data on ground-state properties can only constrain a very limited set of terms and parameters in a general expansion of the nuclear EDF. Until recently the standard procedure of adjusting nuclear density functionals was to perform a least-squares fit of parameters simultaneously to empirical properties of symmetric and asymmetric nuclear matter, and to selected ground-state data of a small set of spherical closed-shell nuclei. A new generation of density functionals is currently being developed that, on the one hand, is more firmly constrained by microscopic treatments of effective inter-nucleon interactions and, on the other hand, their parameters are adjusted to much larger data sets of ground-state properties, including both spherical and deformed nuclei. Methods of statistical analysis can be used to assess the uniqueness and predictive power of particular functionals, as well as the stability or sensitivity of model parameters. These methods can also be used to determine the type of data that better constrain model parameters.

In this work we have analyzed a particular class of relativistic energy density functionals characterized by contact (point-coupling) effective nucleon-nucleon interactions and density-dependent coupling parameters. The “best-fit model”, the functional DD-PC1, was adjusted in a multistep parameter fit to experimental masses of a large set of deformed heavy nuclei. We have used covariance analysis to examine the stability of this functional in nuclear matter, and to determine weakly and strongly constrained combinations of parameters. In particular, instead of analyzing uncertainties and correlations between the individual parameters of the given functional, we have examined correlations between the lowest-order terms in a Taylor expansion of the density-dependent coupling parameters around the saturation point in nuclear matter. To this end, we have produced a set of pseudo-observables in infinite and semi-infinite nuclear matter, computed with the functional DD-PC1, and used these data to compose a quality measure  $\chi^2$ . In the spirit of statistical analysis, we have analyzed the behavior of  $\chi^2$  around the minimum. In particular, we have computed uncertainties of model parameters and correlation coefficients between parameters, as well as the eigenvectors and eigenvalues of the matrix of second derivatives of  $\chi^2$ . This has allowed to determine stiff and soft directions in the parameter space, that is, to deduce which combinations of model parameters are firmly constrained by nuclear matter pseudo-data, and which combinations are poorly determined by the quality measure  $\chi^2$ . In addition, we have also analyzed the uncertainties of observables that were not included in the calculation of  $\chi^2$ : binding energy of asymmetric nuclear matter, surface thickness of semi-infinite nuclear matter, binding energies and charge radii of finite nuclei. The present covariance analysis has shown that, even though the functional DD-PC1 has been successfully employed in a series of spectroscopic studies and used to predict various nuclear properties, several combinations of model parameters appear

to be weakly constrained in nuclear matter and some of them produce rather large uncertainties for observables of finite nuclei. The results of this analysis also show that the adopted ansatz for the density dependence of the coupling parameters of DD-PC1 should be reexamined.

More generally, the results obtained in this work illustrate how a simple analysis of the quality measure  $\chi^2$  around the minimum in nuclear matter can be used as a starting point in the determination of the functional density dependence of a nuclear EDF, and in the selection of the type of data that can more firmly constrain the values of model parameters.

## References

- [1] S. Brandt. *Statistical and computational methods in data analysis*. Springer, New York, 1997.
- [2] T. Nikšić, D. Vretenar, and P. Ring. *Phys. Rev. C*, 78:034318, 2008.
- [3] M. Bender, P.-H. Heenen, and P.-G. Reinhard. *Rev. Mod. Phys.*, 75:121, 2003.
- [4] B. D. Serot and J. D. Walecka. *Adv. Nucl. Phys.*, 16:1–316, 1986.
- [5] P.-G. Reinhard, M. Rufa, J. A. Maruhn, W. Greiner, and J. Friedrich. *Z. Phys. A*, 323:13–25, 1986.
- [6] J. Friedrich and P.-G. Reinhard. *Phys. Rev. C*, 33:335, 1986.
- [7] P.-G. Reinhard. *Rep. Prog. Phys.*, 52:439–514, 1989.
- [8] P. Ring. *Prog. Part. Nucl. Phys.*, 37:193–263, 1996.
- [9] D. Vretenar, A.V. Afanasjev, G.A. Lalazissis, and P. Ring. *Phys. Rep.*, 409:101, 2005.
- [10] S. G. Zhou S. Q. Zhang W. H. Long J. Meng, H. Toki and L. S. Geng. *Prog. Part. Nucl. Phys.*, 57:470, 2006.
- [11] B. A. Nikolaus, T. Hoch, and D. G. Madland. *Phys. Rev. C*, 46:1757, 1992.
- [12] T. Bürvenich, D. Madland, J. A. Maruhn, and P.-G. Reinhard. *Phys. Rev. C*, 65:044308, 2002.
- [13] S. Typel and H. H. Wolter. *Nucl. Phys. A*, 656:331, 1999.
- [14] J. Piekarewicz, B. K. Agrawal, G. Colò, W. Nazarewicz, N. Paar, P.-G. Reinhard, X. Roca-Maza, and D. Vretenar. *Phys. Rev. C*, 85:041302, 2012.
- [15] P.-G. Reinhard, J. Piekarewicz, W. Nazarewicz, B. K. Agrawal, N. Paar, and X. Roca-Maza. *Phys. Rev. C*, 88:034325, 2013.
- [16] F.J. Fattoyev and J. Piekarewicz. *Phys. Rev. C*, 84:064302, 2011.
- [17] P.-G. Reinhard and W. Nazarewicz. *Phys. Rev. C*, 81:051303, 2010.
- [18] J. Dobaczewski, W. Nazarewicz, and P.-G. Reinhard. Error estimates of theoretical models: a guide. *J. Phys. G*, 41, 2014.
- [19] L.F. Richardson and J. A. Gaunt. *Phil. Trans. R. Soc. Lond. A*, 226:299, 1927.
- [20] Y. Gao, J. Dobaczewski, M. Kortelainen, J. Toivanen, and D. Tarpanov. *Phys. Rev. C*, 87:034324, 2013.
- [21] J. W. Negele and D. Vautherin. Density–matrix expansion for an effective nuclear hamiltonian. *C5:1472–1492*, 1972.
- [22] P.-G. Reinhard and C. Toepffer. Correlations in nuclei and nuclear dynamics. *Int. J. Mod. Phys. E*, 3:435–521, 1994.
- [23] R M Dreizler and E K U Gross. *Density Functional Theory: An Approach to the Quantum Many-Body Problem*. Springer-Verlag, Berlin, 1990.
- [24] H.-P. Duerr. Relativistic effects in nuclear forces. *Phys. Rev.*, 103:469–480, 1956.
- [25] M. Jaminon and C. Mahaux. *Phys. Rev. C*, 40:354, 1989.
- [26] M. Jaminon and C. Mahaux. *Phys. Rev. C*, 41:697, 1990.
- [27] T. Nikšić, D. Vretenar, and P. Ring. *Prog. Part. Nucl. Phys.*, 66:519, 2011.